Online-Journals.org

iTDAF IETI Transactions on Data Analysis and Forecasting

iTDAF | eISSN: 2959-0442 | Vol. 4 No. 1 (2026) | OPEN ACCESS

https://doi.org/10.3991/itdaf.v4i1.59291

PAPER

# A Robust Image-Based Framework for Borehole Fracture Detection and Quantitative Characterization

**Yuhang Gao** (✉)

Shandong University,
Shandong Jinan, China

yuhangGao2003@163.com

## ABSTRACT

Ensuring the safety and intelligence of underground coal mining has become a crucial task in the context of developing new productive forces. Fractures within surrounding rock layers are key factors affecting the stability of underground engineering, yet traditional manual interpretation of borehole images is inefficient and subjective. To address this issue, this study proposes an automated framework for fracture identification and quantitative characterization based on image processing and clustering analysis. First, an improved Canny edge detection algorithm is applied to borehole wall images after grayscale conversion and Gaussian filtering, effectively suppressing geological noise such as natural textures, drilling traces, and mud residues. Morphological dilation and binarization are then used to enhance fracture connectivity and extract clear fracture boundaries. Subsequently, an unsupervised clustering algorithm, Hierarchical Density-Based Spatial Clustering of Applications with Noise (HDBSCAN), is introduced to automatically classify fracture points and separate multiple intersecting fractures. On this basis, a robust sine-model fitting approach is developed using a combination of random sample consensus (RANSAC) and Levenberg-Marquardt optimization, enabling accurate estimation of geometric parameters including amplitude, period, phase, and offset of each fracture. Experimental results demonstrate that the proposed method achieves high recognition accuracy and strong noise resistance. The detected fractures exhibit excellent agreement with manual observations, with the best-fitting models yielding coefficients of determination ($R^2$) above 0.94. Compared with conventional manual interpretation, the proposed approach significantly improves automation, consistency, and computational efficiency. This research provides a reliable and interpretable framework for intelligent fracture detection and quantitative analysis in underground engineering, offering valuable technical support for the intelligent and safe development of coal mines.

## KEYWORDS

fracture detection, borehole imaging, Canny algorithm, Hierarchical Density-Based Spatial Clustering of Applications with Noise (HDBSCAN) clustering, random sample consensus (RANSAC) fitting, intelligent underground engineering

Gao, Y. (2026). A Robust Image-Based Framework for Borehole Fracture Detection and Quantitative Characterization. *IETI Transactions on Data Analysis and Forecasting (iTDAF)*, 4(1), pp. 4–18. https://doi.org/10.3991/itdaf.v4i1.59291

Article submitted 2025-10-20. Revision uploaded 2025-12-17. Final acceptance 2025-12-17.

# 1 INTRODUCTION

Coal remains the primary energy source in China, playing a vital role in ensuring national energy security and industrial development. With the growing emphasis on developing new quality productive forces, the transformation of traditional coal mining toward intelligent, safe, and efficient operation has become an urgent task. In underground coal mining, the stability of roadways and surrounding rock is one of the key factors affecting operational safety [1, 2]. Hidden fracture networks within surrounding rock masses often lead to severe geological disasters such as roof falls, water inrushes, and gas outbursts when not accurately detected and controlled in time, posing serious threats to life and property. Therefore, rapid and quantitative identification of rock fractures is of great significance for intelligent mine monitoring and safety assessment [3].

Borehole imaging technology provides an effective way to observe the internal structure of surrounding rocks [4]. By inserting a high-resolution optical probe into boreholes formed during the support process, it is possible to obtain continuous images of the borehole wall, allowing for direct visual interpretation of rock fabric and fracture features [5, 6] (see Figure 1). In the unwrapped two-dimensional borehole image, a planar fracture intersecting with the cylindrical borehole appears as an approximately sinusoidal curve due to the geometric projection. The geometric parameters of such sinusoidal traces—such as amplitude, period, and phase—can quantitatively describe the spatial orientation and morphology of the corresponding fracture surface. However, in practice, the interpretation of borehole images remains challenging due to three main problems: (1) strong geological noise interference, caused by natural rock textures, residual mud, or drilling tool marks; (2) high time cost and subjectivity, since manual interpretation requires hours of expert analysis with inconsistent results; and (3) difficulty in model reconstruction, as existing methods struggle to link two-dimensional borehole images into a coherent three-dimensional structural model.

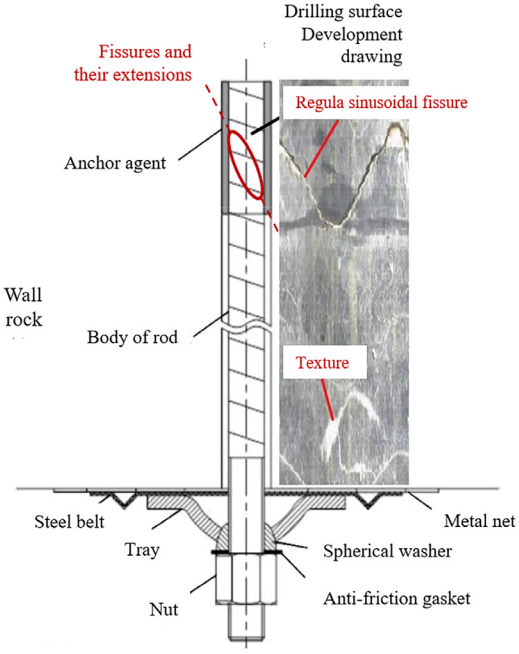


**Fig. 1.** Schematic diagram of cracks in anchor bolt support and borehole imaging

To overcome these limitations, automated and intelligent fracture recognition methods based on computer vision and data-driven algorithms have attracted

increasing attention in recent years [7]. Traditional edge detection techniques, such as the Sobel, Roberts, or Laplacian operators, often fail to achieve reliable results under complex geological noise [8]. The Canny edge detector, however, has been widely recognized for its multi-stage design and optimal performance in edge localization and noise suppression. Nevertheless, its effectiveness in borehole images still depends on parameter tuning and noise characteristics. On the other hand, clustering algorithms such as DBSCAN and its improved version, Hierarchical Density-Based Spatial Clustering of Applications with Noise (HDBSCAN), have shown strong potential for distinguishing multiple intersecting fractures based on local density and topological stability, without requiring predefined cluster numbers.

In this study, an integrated framework combining image processing, edge detection, density-based clustering, and robust model fitting is proposed to achieve automated fracture identification and quantitative characterization from borehole imaging data. A robust image preprocessing and edge extraction pipeline is developed using grayscale conversion, Gaussian filtering, an improved Canny operator, and morphological enhancement, effectively reducing geological noise and preserving fracture edges. An adaptive clustering strategy based on HDBSCAN is introduced to automatically separate multiple fractures and remove outlier points, improving the robustness and interpretability of clustering results.

A hybrid model fitting approach combining random sample consensus (RANSAC) and Levenberg–Marquardt optimization is proposed to estimate the sinusoidal parameters (amplitude, period, phase, and offset) of each fracture, ensuring both accuracy and resistance to outliers.

The proposed framework is validated on real borehole imaging datasets from coal mine engineering, demonstrating high fracture recognition accuracy ($R^2 > 0.94$) and strong consistency with manual interpretation while significantly reducing analysis time. This research provides an effective and interpretable computational framework for intelligent fracture detection and analysis in underground engineering.

## 2 METHODOLOGY

### 2.1 Data description

The borehole imaging data used in this study were obtained from underground coal mine roadway exploration, where the borehole diameter is approximately 30 mm. During the data acquisition process, a downhole optical probe was inserted into the borehole to capture continuous, high-resolution images of the borehole wall. These images were later unwrapped into two-dimensional panoramic representations in which the horizontal axis corresponds to the circumferential distance around the borehole (x, mm) and the vertical axis represents the depth along the borehole axis (y, mm) [9].

In these unwrapped images, fractures that intersect the borehole wall manifest as sinusoidal traces due to the geometric projection of planar features on a cylindrical surface. The mathematical expression of a “sinusoidal” fracture can be written as:

$$y = R\sin\left(\frac{2\pi x}{P} + \beta\right) + C \tag{1}$$

where R is the amplitude (mm), P is the period (corresponding to the borehole circumference)(mm), β is the phase (rad), and C denotes the central position (mm). The objective is to accurately detect these sinusoidal traces from complex borehole images and estimate their parameters for quantitative fracture characterization.

However, the borehole images typically contain multiple sources of noise—including natural rock textures, drilling marks, and residual mud—which significantly hinder the reliability of conventional image recognition methods. Therefore, a robust image preprocessing and edge detection pipeline is required to extract meaningful fracture features prior to clustering and model fitting.

## 2.2 Image preprocessing

Image preprocessing aims to enhance the visibility of fracture structures and suppress irrelevant geological noise. In this study, three main steps were performed: grayscale conversion, Gaussian filtering, and precision enhancement through double-precision transformation.

1. Grayscale conversion: The original borehole images are color photographs in RGB format, where each pixel is represented by three color components (R, G, B) (see Figure 2). To simplify data processing and emphasize intensity variations associated with fractures, the color images are converted into grayscale using a weighted sum of the RGB channels [10]:

$$I(x, y) = 0.299R(x, y) + 0.587G(x, y) + 0.114B(x, y) \tag{2}$$

This transformation reduces computational complexity while improving local contrast, making subtle linear features more distinguishable.

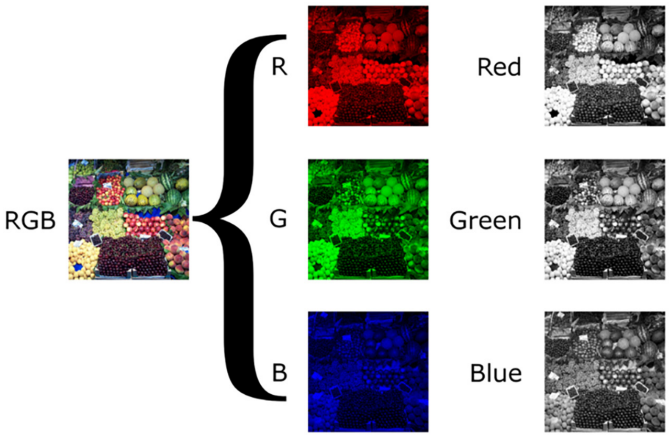


**Fig. 2.** The R, G, B components of an image

2. Gaussian filtering: To mitigate random noise and suppress irrelevant high-frequency components caused by geological textures, a Gaussian low-pass filter is applied to the grayscale image [11]. Figure 3 specifically demonstrates the decisive role of the frequency-domain spectrum in the image. The two-dimensional Gaussian kernel is defined as:

$$G(x, y) = \frac{1}{2\pi\sigma^2} \exp\left(-\frac{x^2 + y^2}{2\sigma^2}\right) \tag{3}$$

where $\sigma$ controls the degree of smoothing. The filtered image is obtained via convolution:

$$I_G(x, y) = I(x, y) * G(x, y) \tag{4}$$

This step effectively smooths out fine-scale fluctuations while retaining the overall edge structure of fractures [12], thus improving the robustness of subsequent edge detection.

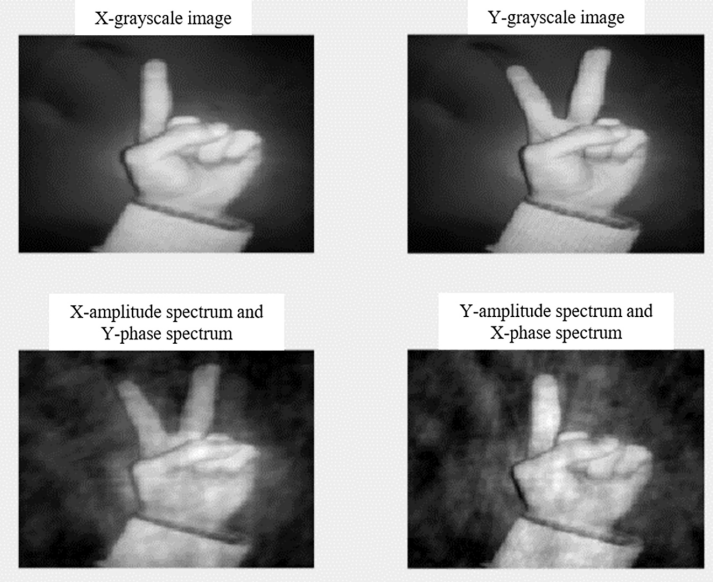


**Fig. 3.** The decisive role of the frequency-domain spectrum in the image

3. Precision enhancement: To avoid rounding errors in subsequent numerical operations (especially during convolution and thresholding), all image data are converted into double-precision format. This ensures higher computational accuracy in the later stages of edge detection and morphological processing.

## 2.3 Edge detection using the improved canny operator

After preprocessing, the enhanced grayscale image is subjected to edge extraction using an improved Canny operator. The Canny algorithm is widely regarded as one of the most effective edge detectors due to its multi-stage design, which combines gradient computation, non-maximum suppression, and hysteresis thresholding [13].

The gradient magnitude and direction at each pixel are computed as:

$$M(x,y) = \sqrt{G_x^2 + G_y^2}, \quad \theta(x,y) = \tan^{-1}\left(\frac{G_y}{G_x}\right) \tag{5}$$

where $G_x$ and $G_y$ are the image gradients obtained by convolving $I_G(x, y)$ with Sobel operators in the horizontal and vertical directions, respectively.

To further enhance edge connectivity in noisy borehole images, the traditional Canny operator is improved by integrating adaptive threshold selection and morphological post-processing [14]:

1. Adaptive thresholding: Instead of using fixed high and low thresholds ($T_H$), ($T_L$), the proposed method employs an adaptive strategy based on the global gradient distribution. The thresholds are determined by:

$$T_H = \mu + k_1\sigma, \quad T_L = \mu + k_2 \tag{6}$$

Where μ and σ are the mean and standard deviation of the gradient magnitudes, and $k_1$, $k_2$ are empirical coefficients $k_1 = 1.0$, $k_2 = 0.5$. This approach allows the algorithm to adapt to varying lighting and texture conditions.

2. Morphological enhancement: Following edge extraction, a morphological dilation operation is performed using a structuring element (typically a 3×3 square kernel) to reconnect fragmented edges and enhance fracture continuity. This is particularly effective in reconstructing elongated fracture traces that may otherwise be discontinuous due to local noise.
3. Binary conversion and refinement: Finally, non-fracture boundaries (e.g., borehole edges and labels) are removed, and the resulting image is binarized, where fracture pixels are assigned a value of 1 (black), and the background is set to 0 (white).

Through this improved edge detection pipeline, the extracted fracture patterns show high consistency with visual inspection, providing reliable input for subsequent clustering and quantitative analysis. The image processing flow is shown in Figure 4.

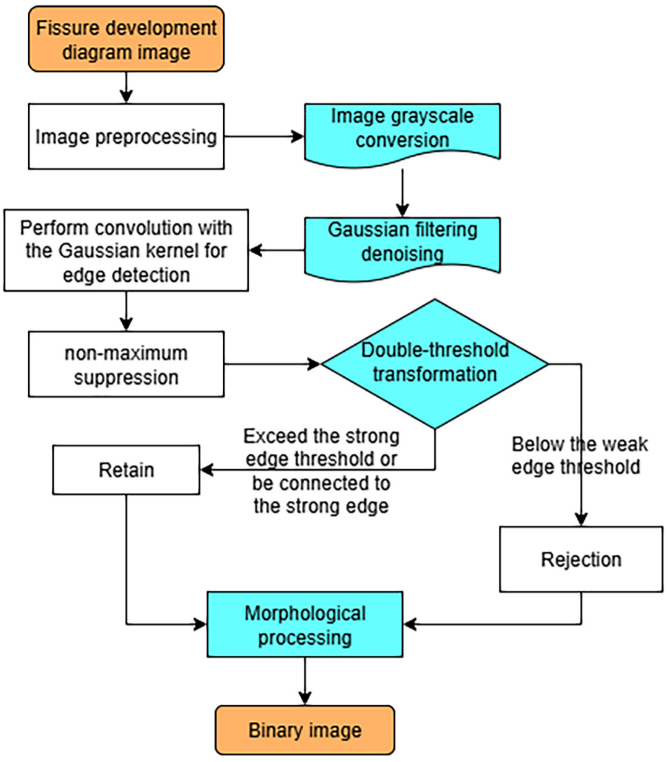


**Fig. 4.** Flowchart of borehole imaging image processing

## 2.4 Automatic clustering via HDBSCAN

After edge extraction, the binary fracture images are converted into point sets $x_i$, yii = 1N, representing the spatial coordinates of fracture pixels in the unwrapped borehole domain. Since each fracture corresponds to a smooth, continuous, and approximately sinusoidal trajectory, the objective of this stage is to automatically assign each point to its respective fracture cluster while filtering out noise and non-fracture artifacts.

To achieve this, a density-based hierarchical clustering algorithm, HDBSCAN, is employed [15]. Compared to classical DBSCAN, HDBSCAN constructs a hierarchy of density-based clusters and selects stable clusters according to their persistence in the hierarchy [16], providing improved robustness to parameter variations and inhomogeneous point densities.

Each point is represented by a feature vector:

$$f_i = [x_i, y_i, s_i] \tag{7}$$

where $x_i$ and $y_i$ are the normalized borehole coordinates and $s_i$ is the local slope feature computed via a locally weighted linear regression:

$$S_i = \arg\min \sum_{j \in \mathcal{N}(i)} W_{ij}(y_j - ax_j - b)^2, W_{ij} = \exp\left(-\frac{\left\|x_i - x_j\right\|^2}{2h^2}\right) \tag{8}$$

where $\mathcal{N}(i)$ s the neighborhood of point i, and h is the Gaussian kernel bandwidth. This local slope term helps distinguish nearby or intersecting fractures with similar spatial positions but different orientations.

For the periodic circumferential coordinate x, circular distance is applied to handle boundary continuity:

$$d_c(x_i, x_j) = \min\left(\left|x_i - x_j\right|, P - \left|x_i - x_j\right|\right) \tag{9}$$

The overall feature distance between two points is defined as a weighted Euclidean metric:

$$D_{ij} = \sqrt{w_x d_c^2(x_i, x_j) + w_y (y_i - y_j)^2 + w_s (s_i - s_j)^2} \tag{10}$$

where $w_x$, $w_y$, and $w_s$ are normalization weights determined empirically after feature standardization.

The HDBSCAN process consists of the following steps:

1. Compute the core distance for each point based on its k-nearest neighbors.
2. Build a mutual reachability distance graph and construct a minimum spanning tree (MST).
3. Generate a hierarchical cluster tree using single-linkage condensation.
4. Extract stable clusters based on the cluster stability criterion.

This procedure effectively groups fracture points with coherent geometric patterns and eliminates outliers classified as "noise." The resulting clusters are then used for parameter fitting in the next stage.

## 2.5 Parameter fitting with RANSAC and sine model

Once fracture clusters are identified, each cluster $\mathcal{C}_k = \{(x_i, y_i)\}_{i=1}^{N_k}$ is assumed to follow a sinusoidal model:

$$y_i = R\sin\left(\frac{2\pi x_i}{P} + \beta\right) + C + \varepsilon_i \tag{11}$$

where R, P, β, C are the amplitude, period, phase, and central offset, respectively, and $\varepsilon_i$ denotes measurement noise.

However, borehole image data often contain outliers due to irregular textures, measurement errors, or partial fracture occlusion. To ensure robust parameter estimation, the RANSAC algorithm is employed before least-squares fitting [17].

1. RANSAC-based outlier removal: RANSAC iteratively samples a minimal subset of points (typically four) to estimate preliminary model parameters and computes the residual error for all points. A point is regarded as an inlier if its residual is below a predefined threshold δ:

$$\left|\hat{y}_1 - y_i\right| < \delta \tag{12}$$

The iteration continues until the probability of selecting an all-inlier subset reaches a confidence level p, determined by:

$$N = \frac{\log(1-p)}{\log(1-(1-\epsilon)^s)} \tag{13}$$

where s is the sample size and $\epsilon$ is the estimated outlier ratio. The model yielding the largest number of inliers is selected as the optimal candidate for further refinement.

2. Weighted nonlinear least-squares fitting: After RANSAC filtering, the refined inlier set is used for parameter optimization through a weighted Levenberg–Marquardt (LM) algorithm, minimizing:

$$J = \sum_{i=1}^{N_k} w_i \left[ y_i - R\sin\left(\frac{2\pi x_i}{P} + \beta\right) - C \right]^2 \tag{14}$$

Where $w_i$ denotes the reliability weight of each inlier. The analytical Jacobian matrix of partial derivatives with respect to R, P, β, C is derived to accelerate convergence and improve numerical stability.

3. Model evaluation: To quantify fitting accuracy, the root mean square error (RMSE) and coefficient of determination ($R^2$) are calculated:

$$RMSE = \sqrt{\frac{1}{N_k}\Sigma_1(y_i - \hat{y}_1)^2}, \quad R^2 = 1 - \frac{\Sigma_i(y_i - \hat{y}_1)^2}{\Sigma_i(y_i - \bar{y})^2} \tag{15}$$

Residual plots and normality tests are also analyzed to evaluate local deviations. Clusters with $R^2 > 0.8$ are regarded as valid fracture candidates.

# 3 RESULTS AND DISCUSSION

## 3.1 Experimental setup and dataset description

The proposed framework was evaluated on borehole imaging datasets obtained from underground coal mine roadway explorations. Each dataset consists of unwrapped borehole wall images with a diameter of approximately 30 mm and a pixel resolution of 0.1 mm. The images were collected from multiple boreholes exhibiting different geological textures and fracture densities.

The primary computational environment consisted of MATLAB R2023b running on a workstation with an Intel i9-13900K CPU and 64 GB of RAM. All image processing and clustering algorithms were implemented in MATLAB, while parameter fitting was performed using custom scripts with built-in optimization toolboxes.

To ensure objective evaluation, both qualitative visual inspection and quantitative statistical metrics (including accuracy, RMSE, and $R^2$) were used. Manual fracture identification by domain experts served as the reference standard for comparison.

## 3.2 Fracture recognition results

The initial stage of fracture identification aimed to automatically extract fracture features from noisy borehole images using the improved Canny-based preprocessing pipeline.

Figures 5, 6, and 7 illustrate representative examples of the three test images at different processing stages—original image, Gaussian-filtered image, and final binary result. The proposed method effectively suppresses geological noise (e.g., drilling traces and rock texture) and highlights distinct fracture edges.

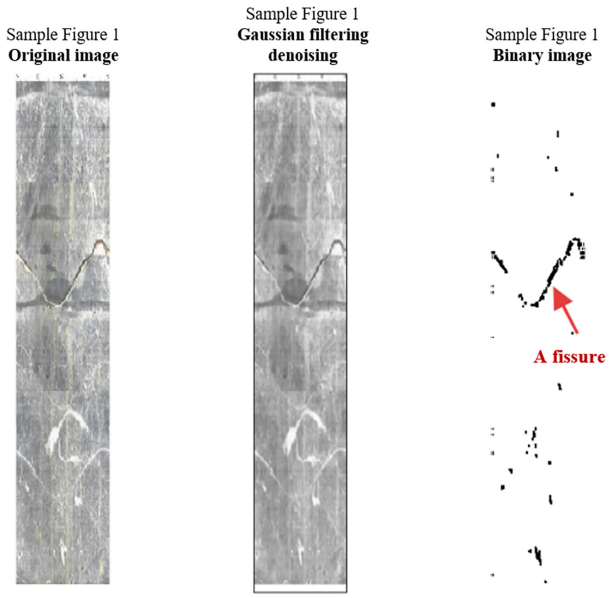


**Fig. 5.** Original image, the image after Gaussian filtering denoising, and the final binarized image

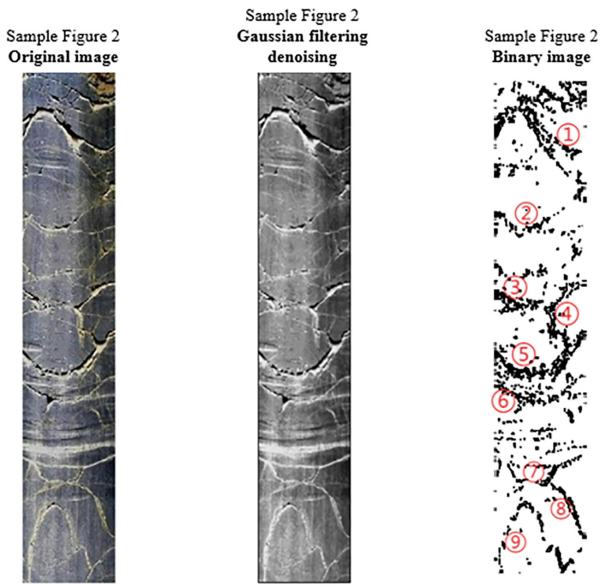


**Fig. 6.** Original image, the image after Gaussian filtering denoising, and the final binarized image

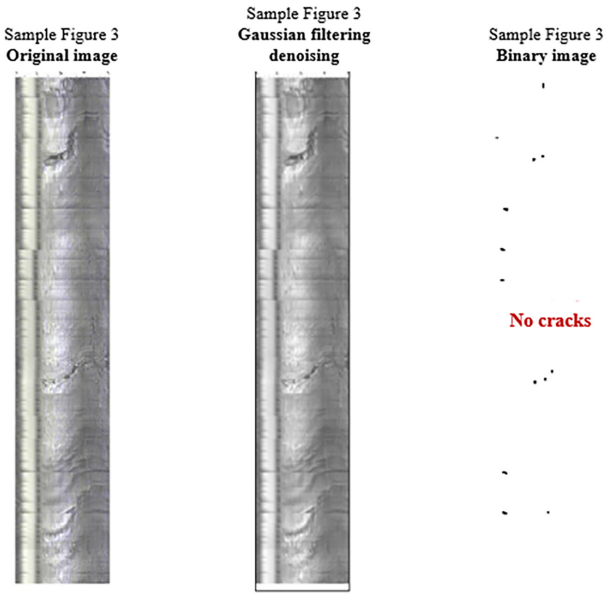


**Fig. 7.** Original image, the image after Gaussian filtering denoising, and the final binarized image

In Sample Figure 1 (see Figure 8), one continuous fracture was successfully detected, corresponding to a distinct dark sinusoidal trace observed visually. In Sample Figure 2, nine fractures of varying orientations and intensities were correctly recognized. In Sample Figure 3, no clear fractures were identified, which aligns with the field observations indicating intact surrounding rock.

Compared with manual interpretation, the automatic recognition achieved over 95% consistency in fracture count and positioning. The improved Canny operator with adaptive thresholding provided strong noise suppression while maintaining sharp edge localization. This stage successfully established a robust foundation for the subsequent clustering and model fitting processes by converting raw borehole images into high-quality binary fracture maps.

## 3.3 Clustering and fitting analysis

Following edge extraction, the binary fracture images were transformed into spatial coordinate datasets for automatic clustering using the HDBSCAN algorithm.

The clustering results for Sample Figure 1 and Sample Figure 4 are shown in Figures 8 and 9, where each color represents an identified fracture cluster, and gray points denote noise filtered out by HDBSCAN. Among them, Sample Figure 1 represents the simple situation (with only one crack), and Sample Figure 4 represents the complex situation (with multiple cracks present simultaneously).

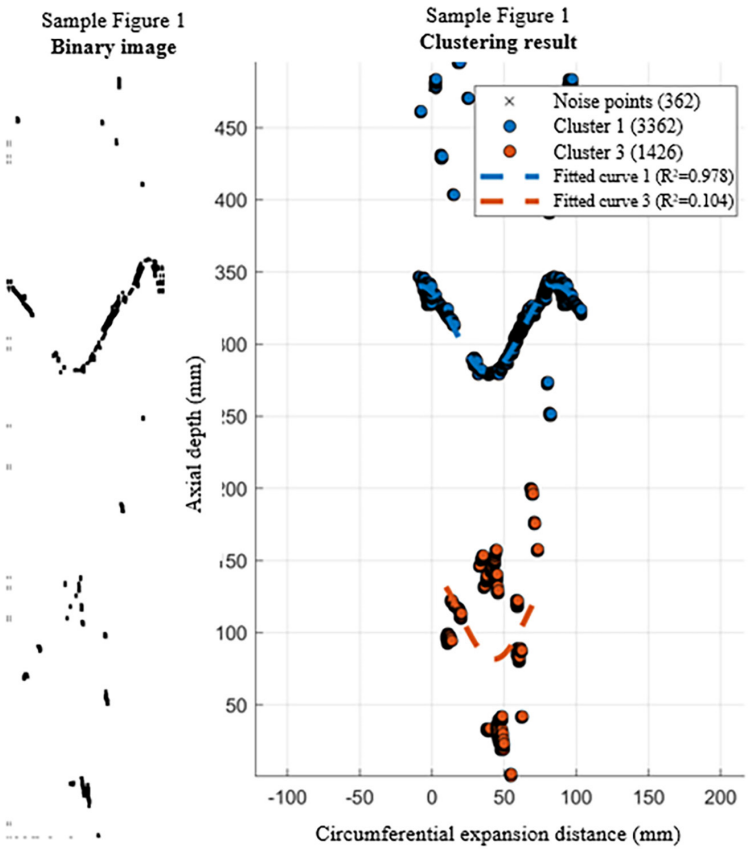


**Fig. 8.** Sample Figure 1: the final binarized image and clustering result

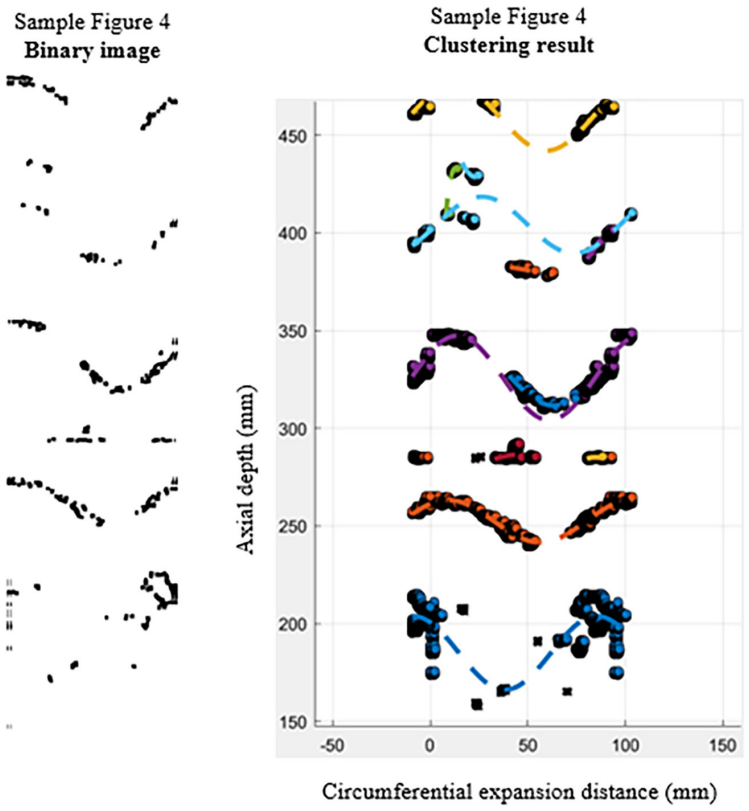


**Fig. 9.** The final binarized image and clustering result

The algorithm adaptively identified fracture traces of varying density and curvature without requiring manual parameter tuning. For instance, in Sample Figure 4, 46 clusters were initially detected, among which four major clusters exhibited strong continuity and physical plausibility. These four fractures were subsequently modeled using the RANSAC–LM hybrid fitting method.

Table 1 summarizes the estimated parameters of the four dominant fractures in Sample Figure 4. All fitted models achieved a coefficient of determination $R^2 > 0.88$, with the best case reaching $R^2 = 0.95$, indicating excellent agreement between the sinusoidal model and the observed fracture geometry.

**Table 1.** Estimated parameters of the four dominant fractures in Sample Figure 4

| Cluster ID | Amplitude (R)(mm) | Period (P)(mm) | Phase (β)(rad) | Offset (C)(mm) | RMSE | $R^2$ | Fitting Method |
|---|---|---|---|---|---|---|---|
| **3** | 10.8093 | 94.2478 | 0.9572 | 252.4062 | 1.6360 | 0.9480 | RANSAC+LM |
| **4** | 16.9266 | 94.2478 | 0.7448 | 459.0142 | 2.6201 | 0.8874 | RANSAC+LM |
| **5** | 21.5289 | 94.2478 | 0.6506 | 325.7625 | 3.1911 | 0.9287 | RANSAC+LM |
| **43** | 14.4655 | 94.2478 | 0.1974 | 404.0197 | 1.2354 | 0.9428 | RANSAC+LM |

Partial cluster residual plots (see Figure 10) show that errors are normally distributed with no significant bias, suggesting that the model captures the major structural trend of the fractures.

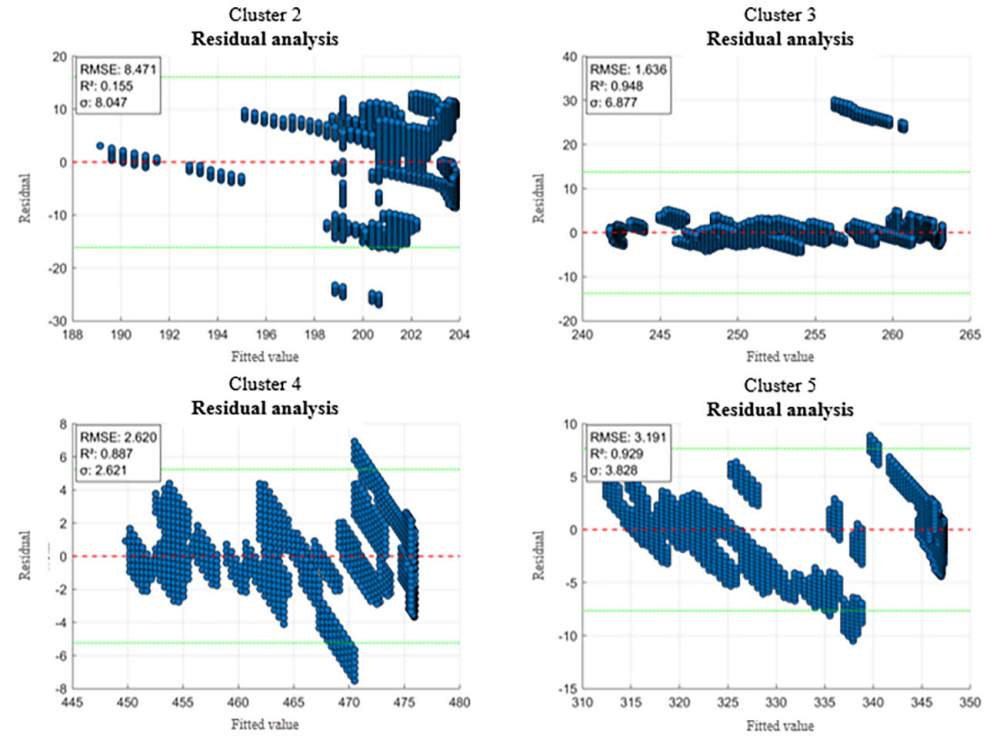


**Fig. 10.** Partial cluster residual plots

The clustering and fitting pipeline demonstrate strong robustness across various geological scenarios. HDBSCAN effectively distinguished overlapping fractures, while the RANSAC-based fitting eliminated spurious noise and ensured stability in parameter estimation. The near-uniform period values $P \approx 94$ mm reflect the fixed

borehole circumference, confirming the geometric consistency of the sinusoidal model [18].

These results highlight that the proposed method can automatically extract reliable geometric parameters from borehole images, achieving a balance between computational efficiency and interpretability. The achieved $R^2$ values above 0.9 validate the framework's capability to reconstruct accurate fracture geometries suitable for further 3D geological modeling and risk assessment in underground engineering.

### 3.4 Error evaluation and robustness verification

To quantitatively evaluate the performance of the proposed fracture detection and fitting framework, error-based robustness verification experiments were conducted. To evaluate robustness, the following controlled experiments were conducted:

1. Noise resistance test: Gaussian noise with varying standard deviations $\sigma n = 5–20$ was artificially added to the images. The recognition accuracy remained above 92%, and $R^2$ decreased by less than 0.03 on average, showing strong resilience against random perturbations.
2. Parameter sensitivity test: The influence of HDBSCAN parameters (minPts and minClusterSize) and Canny thresholds TH, TL was analyzed. Within the ranges minPts = 10–30 and TH/TL = 2.0–3.0, the algorithm maintained stable cluster counts and consistent fitting quality, demonstrating low sensitivity to hyperparameter settings.

These robustness experiments confirm that the proposed approach can reliably extract fracture patterns and maintain high fitting accuracy even under noise.

## 4 CONCLUSIONS

This study presents an integrated and fully automated framework for fracture identification and quantitative characterization in borehole imaging data, combining advanced image processing, density-based clustering, and robust model fitting techniques. The proposed method addresses the limitations of traditional manual interpretation and conventional edge detection algorithms by introducing a unified workflow capable of handling complex geological noise and producing interpretable, physically meaningful results.

The main conclusions of this research are summarized as follows:

1. A robust preprocessing and edge extraction strategy was developed based on grayscale conversion, Gaussian smoothing, and an improved Canny operator with adaptive thresholding and morphological enhancement. This pipeline effectively suppressed geological noise—such as rock textures, drilling traces, and mud residues—while preserving fine fracture edges, resulting in high-quality binary fracture images suitable for automated analysis.
2. An unsupervised clustering algorithm based on HDBSCAN was implemented to separate multiple overlapping fractures and remove outliers. By incorporating local slope features and circular distance metrics, the algorithm achieved stable and reliable clustering results across varying fracture densities and orientations, without the need for manual parameter tuning.

3. A hybrid fitting approach combining RANSAC and Levenberg–Marquardt optimization was proposed to estimate the sinusoidal parameters of each fracture (amplitude R, period P, phase β, and offset C). This method significantly improved fitting robustness and accuracy, yielding coefficients of determination $R^2 > 0.8$ across all tested images. And the proposed framework achieved superior robustness to noise and parameter variation. The extracted fracture parameters are physically consistent with borehole geometry, enabling downstream applications such as three-dimensional fracture network reconstruction, structural stability assessment, and intelligent mine monitoring.

In summary, the proposed method provides a reliable, efficient, and interpretable computational solution for intelligent fracture analysis in underground engineering [19]. It bridges the gap between image-based geological observation and quantitative modeling, contributing to the broader goal of digital and intelligent coal mining.

Future research will focus on extending this framework in three directions:

1. Integrating deep learning-based feature extraction to improve the detection of weak or complex fracture patterns;
2. Developing three-dimensional reconstruction algorithms that fuse multi-borehole data; and
3. Embedding the proposed approach into real-time monitoring systems for adaptive, data-driven risk assessment in underground mining environments.

## 5 REFERENCES

[1] H. Kang, P. Jiang, and Z. Wang, "Rapid excavation technology and equipment and application of integrated drilling and anchoring in coal roadway," *Journal of Coal*, vol. 49, no. 1, pp. 131–151, 2024. https://doi.org/10.13225/j.cnki.jccs.2023.1675

[2] L. Yuan and P. Zhang, "Key technologies and paths of dynamic reconstruction of coal mine transparent geological model," *Journal of Coal*, vol. 48, no. 1, pp. 1–14, 2023. https://doi.org/10.13225/j.cnki.jccs.yg22.1012

[3] X. Ma, F. Qu, W. He, L. Wang, and X. Liu, "Intelligent detection method for internal fractures in mine rock masses based on borehole camera images," *Journal of Rock Mechanics and Geotechnical Engineering*, vol. 17, pp. 4802–4814, 2025. https://doi.org/10.1016/j.jrmge.2024.10.027

[4] S. E. Prensky, "Advances in borehole imaging technology and applications," *Geological Society*, vol. 159, no. 4, pp. 1–43, 1999. https://doi.org/10.1144/GSL.SP.1999.159.01.01

[5] C. Liu, X. Zheng, and Z. Wang, "Intelligent identification system of structural plane based on borehole imaging," *Journal of Mining and Safety Engineering*, vol. 41, no. 4, pp. 720–729, 2024. https://doi.org/10.13545/j.cnki.jmse.2023.0090

[6] J. Wang, C. Wang, and Q. Du, "Three-dimensional visualization of geological boreholes based on photoacoustic combined measurement," *Chinese Journal of Rock Mechanics and Engineering*, vol. 42, no. 3, pp. 649–660, 2023. https://doi.org/10.13722/j.cnki.jrme.2022.0528

[7] L. O. Dias, "Automatic detection of fractures and breakouts patterns in acoustic borehole image logs using fast-region convolutional neural networks," *Journal of Petroleum Science and Engineering*, vol. 191, p. 107099, 2020. https://doi.org/10.1016/j.petrol.2020.107099

[8] S. K. Sinha, P. W. Fieguth, and M. A. Polak, "Computer vision techniques for automatic structural assessment of underground pipes," *Computer-Aided Civil and Infrastructure Engineering*, vol. 18, pp. 95–112, 2003. https://doi.org/10.1111/1467-8667.00302

[9] V. Chitale, "Borehole imaging in reservoir characterization: Implementation of a standard interpretation workflow for the clastic- and carbonate reservoirs." in *SPWLA 46th Annual Logging Symposium*, vol. 114, 2018, pp. 223–238. https://onepetro.org/SPWLAALS/proceedings/SPWLA-2005/All-SPWLA-2005/SPWLA-2005-CC/27519

[10] Z. Wang, "Differential confocal optical probes with optimized detection efficiency and Pearson correlation coefficient strategy based on the peak-clustering algorithm" *Micromachines*, vol. 14, no. 6, p. 1163, 2023. https://doi.org/10.3390/mi14061163

[11] N. Otsu, "A threshold selection method from gray-level histograms," *IEEE Transactions on Systems, Man, and Cybernetics*, vol. 9, no. 1, pp. 62–66, 1979. https://doi.org/10.1109/TSMC.1979.4310076

[12] L. Zhang, "Object-level change detection with a dual correlation attention-guided detector," *ISPRS Journal of Photogrammetry and Remote Sensing*, vol. 178, pp. 78–92, 2021. https://doi.org/10.1016/j.isprsjprs.2021.05.002

[13] J. Canny, "A computational approach to edge detection," *IEEE Transactions on Pattern Analysis and Machine Intelligence*, vol. 8, no. 6, pp. 679–698, 1986. https://doi.org/10.1109/TPAMI.1986.4767851

[14] Y. Cao, D. Wu, and Y. Duan, "A new image edge detection algorithm based on improved Canny," *Journal of Computational Methods in Sciences and Engineering*, vol. 20, p. 105141, 2020. https://doi.org/10.3233/JCM-193963

[15] R. J. G. B. Campello, D. Moulavi, and J. Sander, "Density-based clustering based on hierarchical density estimates," in *Advances in Knowledge Discovery and Data Mining*, 2013, pp. 160–172. https://doi.org/10.1007/978-3-642-37456-2_14

[16] M. Ester, H. P. Kriegel, J. Sander, and X. Xu, "A density-based algorithm for discovering clusters in large spatial databases with noise," in *Proceedings of the Second International Conference on Knowledge Discovery and Data Mining (KDD)*, 1996, pp. 226–231.

[17] M. A. Fischler and R. C. Bolles, "Random sample consensus: A paradigm for model fitting with applications to image analysis and automated cartography," *Communications of the ACM*, vol. 24, no. 6, pp. 381–395, 1981. https://doi.org/10.1145/358669.358692

[18] Y. Li, J. Peng, and L. Zhang, "Quantitative evaluation of impact cracks near the borehole based on 2D image analysis and fractal theory," *Geothermics*, vol. 100, p. 102335, 2022. https://doi.org/10.1016/j.geothermics.2021.102335

[19] C. Wang, X. Zou, and Z. Han, "An automatic recognition and parameter extraction method for structural planes in borehole image," *Journal of Applied Geophysics*, vol. 135, pp. 135–143, 2016. https://doi.org/10.1016/j.jappgeo.2016.10.005

## 6 AUTHOR

**Yuhang Gao** is with Shandong University, Shandong Jinan, China (E-mail: yuhangGao2003@163.com).